Methane Selective Oxidation on Metal Oxide Catalysts at Low Temperatures with O_2 Using an NO/NO_2 Oxygen Atom Shuttle

I. Tyrone Ghampson[b,c], Sean-Thomas B. Lundin[c], Vibin Vargheese[c], Yasukazu Kobayashi[d], Gregory S. Huff[e], Robert Schlögl[e,f], Annette Trunschke[e], S. Ted Oyama[a,c,g*]

[a]School of Chemical Engineering, Fuzhou University, Fuzhou 350116, China

[b]Department of Applied Chemistry for Environment, Graduate School of Urban Environmental Sciences, Tokyo Metropolitan University, 1-1 Minami-Osawa, Hachioji, Tokyo 192-0397, Japan

[c]Department of Chemical Systems Engineering, The University of Tokyo, 7-3-1 Hongo, Bunkyo-ku, Tokyo 113-8656, Japan

[d]Interdisciplinary Research Center for Catalytic Chemistry, National Institute of Advanced Industrial Science and Technology (AIST), Central 5, 1-1-1 Higashi, Tsukuba, Ibaraki 305-8565, Japan

[e]Fritz-Haber-Institut der Max-Planck-Gesellschaft, Faradayweg 4-6, 14195 Berlin, Germany

[f]Department of Heterogeneous Reactions, Max-Planck-Institut für Chemische Energiekonversion, Stiftstraße 34-36, 45470 Mülheim a. d. Ruhr, Germany

[g]Department of Chemical Engineering, Virginia Tech, Blacksburg, VA 24061, United States

* Corresponding author.
E-mail address: oyama@vt.edu (S. Ted Oyama).

Abstract

Methane oxidation using O_2 over transition metal oxides often requires severe conditions (> 500 °C) to achieve detectable conversion. In this study, NO was used to transfer oxygen atoms from O_2, through the facile gas-phase formation of NO_2 at moderate conditions (0.1 MPa and 300 - 400 °C), to oxidize methane over silica-supported transition metal oxides (VO_x, CrO_x, MnO_x, NbO_x, MoO_x, and WO_x). In situ infrared spectroscopy measurements indicated that the reaction likely proceeded by the formation of surface monodentate nitrate intermediates. These nitrate species were formed by an interaction between adsorbed NO_2 and a surface oxygen atom from the metal oxides. During the reaction, the oxides of vanadium, molybdenum, and tungsten formed formaldehyde and CO_2, whereas the oxides of chromium, manganese, and niobium produced only CO_2. These results are consistent with the known hydrocarbon oxidation chemistry of the elements. Contact time measurements on VO_x/SiO_2 indicated that formaldehyde was a primary product and CO_2 was the final product; conversely, analogous measurements on MnO_x/SiO_2 showed that CO_2 was the sole product. The formaldehyde production rate on VO_x/SiO_2, MoO_x/SiO_2, and WO_x/SiO_2, based on surface sites measured by high temperature oxygen chemisorption, compared favorably to oxygenate production rates for stronger oxidants (N_2O and H_2O_2) reported in the literature.

1.   Introduction

Catalytic selective oxidation has been extensively studied for decades, notably by Jerzy Haber and Robert Grasselli, because of its considerable commercial and scientific relevance [1,2,3]. A number of factors have been found to affect selectivity including the metal-oxygen bond strength, the reducibility of the catalyst, the mode of adsorbate bonding, multifunctionality of active sites, the effect of structure, and the role of adsorbed oxygen, among others. Discussion of these factors has been covered in several books [1,4,5,6] and reviews [7,8,9], with these concepts providing guidelines for the design of efficient selective oxidation systems [7]. For example, the role of adsorbed oxygen, proposed by Bielański and Haber [10,11], has been used to explain selectivity differences in various metal oxides. Adsorbed oxygen species are classified as either nucleophilic, which refers to lattice oxygen ions (O^{2-}) and are considered to be responsible for partial oxidation, or electrophilic, which refers to electron deficient species [12] like oxide (O^-), superoxide (O_2^-), and peroxide (O_2^{2-}) that generally lead to deep oxidation. Although this concept is not all-encompassing, Haber [13] and other researchers [14,15] have provided credible evidence to explain the distinct selectivity behaviors of partial oxidation (e.g. Bi_2O_3-MoO_3) and complete oxidation (e.g. Co_3O_4) catalysts. In the present work, differences in reactivity of methane oxidation over a series of transition metal oxide catalysts are explained by the presence of various types of oxygen.

There has been a considerable research effort on the catalytic methane partial oxidation behavior of metal oxides, with silica-supported MoO_3 [16,17,18,19] and V_2O_5 [20, 21,22,23] catalysts being particularly common. These studies have dealt with the identity of active sites [16,19,20] and the effect of structure [18,22,23,24], which have provided important mechanistic understandings of the reaction. For example, it has been observed that Mo or V species

3

molecularly dispersed on silica support favors formaldehyde formation, and the active oxygen species originates from the lattice metal oxide and not from the gas-phase O_2. However, these findings were largely obtained from investigations conducted at high temperatures (> 500 °C), which complicates any assessment of catalytic activity due to potential contributions from gas-phase reactions. In contrast, the use of an $NO+O_2$ mixture in the current work allowed for dissociation of O_2 and detectable conversion of CH_4 at moderate temperatures ($\leq$ 400 °C), which enabled an examination of intrinsic surface reactivities on a series of metal oxides sans gas-phase reaction contributions.

A number of researchers have studied the catalytic gas-phase oxidation of methane with NO/NO_2 but the studies were conducted mostly at elevated temperatures (> 600 °C) [25,26,27,28,29]. Fierro and coworkers reported that the addition of NO to O_2 increased CH_4 conversion and oxygenate selectivities on V_2O_5/SiO_2, which was attributed to gas-phase reactions promoted by NO as a radical initiator [25,26]. Tabata and coworkers showed that while the use of NO/NO_2 promoted oxygenates formation, the use of MoO_3 [27] or $Cu-ZnO/Al_2O_3$ [28,29] catalysts did not result in appreciable improvements in comparison to the blank reaction. These results indicate the predominance of radical reactions which are difficult to control. In this study, reactivity tests were conducted using a recently developed approach for methane oxidation [30,31,32]. These initial studies found that a mixture of $NO+O_2$ formed NO_2 ($NO + \frac{1}{2} O_2 \rightarrow NO_2$) [33] which acted as an oxygen atom carrier during methane oxidation at moderate conditions. Additionally, activity for partial oxidation appeared to be an innate property of the catalyst, irrespective of the oxidant.

2. Experimental

2.1. Materials

The support used in this study was fumed SiO_2 (Evonik, Aerosil 380 PE, BET surface area 350 m^2 g^{-1}). The chemicals used were NH_4VO_3 (Wako, 99%), $C_2H_2O_4 \cdot 2H_2O$ (Wako, 99.5%), $Cr(NO_3)_3 \cdot 9H_2O$ (Strem, 99%), $Mn(NO_3)_2 \cdot 6H_2O$ (Wako, 98%), 99%), $Nb(HC_2O_4)_5 \cdot xH_2O$ (Alfa Aesar), $(NH_4)_6Mo_7O_{24} \cdot 4H_2O$ (Wako, 99%), and $(NH_4)_6H_2W_{12}O_{40} \cdot xH_2O$ (Aldrich, 99.99%). The gases used were CH_4 (99.999%), 20% O_2/He (certified mixture grade), 6% O_2/He (certified mixture grade), 12% NO/He (certified mixture grade), Ar (99.999%) and H_2 (99.999%), and all were purchased from Tokyo Koatsu Yamazaki Co. Ltd.

2.2. Catalyst preparation

The support was calcined in flowing air (14 μmol s^{-1} g^{-1}) at 500 °C (10 °C min^{-1}) for 4 h and impregnated with each aqueous precursor solution by the incipient wetness impregnation technique. Flow rates in μmol s^{-1} can be converted to cm^3(NTP) min^{-1} by multiplication by 1.5. The solutions were prepared by dissolving the desired metal salt (and oxalic acid in the case of the VO_x sample) in deionized water (2 ml of water per gram of silica) using the ratios in Table S1 (Supplementary Information, SI). Lastly, the impregnated samples were dried in static ambient air at 110 °C for 15 h and then calcined in flowing air (14 μmol s^{-1} g^{-1}) at 500 °C (10 °C min^{-1}) for 5 h.

5

2.3.   Catalyst characterization

Surface areas were obtained by the BET method from nitrogen physisorption measurements at liquid nitrogen temperature using a BELSORP mini II micropore size analyzer. Before the measurements, the samples were degassed at 200 °C for 4 h. X-ray diffraction (XRD) patterns of the calcined samples were obtained with a Rigaku RINT 2400 diffractometer using Cu Kα monochromatized radiation at 45 kV and 100 mA. The oxide samples were used as prepared following calcination at 500 °C and scanned in the 10 to 80° 2θ range with a step size of 0.05°.

Temperature-programmed reduction (TPR) profiles were obtained with a TPD-1-AT apparatus fitted with a quadrupole mass spectrometer. Each sample (0.30 g) was pretreated at 500 °C for 1 h in a 20% O_2/He stream (41 µmol s^{-1}), cooled to 50 °C in Ar flow, and then heated to 800 °C at a rate of 10 °C min^{-1} in H_2 flow (68 µmol s^{-1}) while monitoring the water signal (m/z = 18) signal. The onset of bulk reduction (T_{red}) was used for the pretreatment of samples before oxygen uptake.

Oxygen chemisorption was measured using a standard pulse technique [34,35,36,37] with the same apparatus used for the TPR experiments. Prior to the measurements, 0.30 g of sample was treated in 20% O_2/He flow (41 µmol s^{-1}) at 500 °C for 1 h and reduced in H_2 flow (68 µmol s^{-1}) at T_{red} for 2 h. Uptakes were then determined at T_{red} by injecting calibrated pulses of 5% O_2/He (6.4 µmol of O_2) over the catalysts while monitoring the O_2^+ signal (m/z = 32).

2.4.   Raman spectroscopy

Samples for Raman spectroscopy (12 mg) were placed in a Linkam CCR1000 Raman cell with a quartz window. Samples were pretreated with 14 µmol s^{-1} synthetic air at 500 °C for 2 h,

then cooled to 400 °C in 14 µmol s^{-1} N$_2$ and held for 1 h. Raman spectra were acquired after cooling to 30 °C under 14 µmol s^{-1} N$_2$ flow.

Raman spectra were recorded using an S&I TriVista Raman microscope system consisting of an Olympus BX51 microscope with a 10x objective (NA 0.30) coupled to a Princeton Instruments 750 mm spectrograph with a CCD detector (PyLoN:100BR 100x1340 with eXcelon coating). The excitation source was a 488 nm DPSS laser (Coherent Sapphire SF) with laser power reduced to 0.53 mW using neutral density filters. A Semrock edge filter excluded Rayleigh scattered light. The collected light was focused onto the spectrograph slit (100 µm) by an f/4 apochromatic lens and dispersed by a 600 grooves/mm grating, giving a resolution of about 4 cm^{-1}. Wavenumber accuracy was confirmed using polystyrene as a standard [38].

2.5. Catalyst activity studies

The methane oxidation reaction was conducted at 101 kPa and 300 - 400 °C in a fixed-bed quartz reactor using 0.50 g catalyst samples (600 - 1180 µm particle size). Each catalyst was treated in flowing 20% O$_2$/He (68 µmol s^{-1}) at 500 °C for 1 h before reactivity measurements. A mixture of CH$_4$ (20 kPa), NO (1 kPa) and O$_2$ (1 kPa), balanced by He and Ar, was blended in a manifold and introduced into the reactor at a total flow rate of 68 µmol s^{-1}. The methane-rich condition was chosen to avoid the explosive regime. The effluent from the reactor was analyzed by a gas chromatograph (GC) equipped with a barrier discharge ionization detector (Shimadzu GC-2010) and a Restek Rt$^®$-U-BOND capillary column (30 m × 0.32 mm i.d. × 10 µm film diameter), a GC equipped with a thermal conductivity detector (Shimadzu GC-8A) and a molecular sieve 5A column (3 m × 3 mm i.d), and a Fourier transform infrared (FTIR) spectrometer (JASCO FT/IR-6100) equipped with a long path (15 cm) gas cell and a mercury-cadmium-telluride (MCT) detector with a resolution of 4 cm^{-1}. The analytical units were

7

connected in parallel, and the outlet lines and connections were kept at 100 °C to prevent condensation of products. Measurements were taken after steady-state conditions were reached at the highest temperature and then at decreasing and increasing temperatures to establish catalyst stability. Methane conversion (X_{CH_4}) was calculated by dividing the sum of moles of carbon-containing products to the initial number of moles of methane fed. Total oxygen conversion was calculated as the ratio of the moles of oxygen reacted to the moles of oxygen fed. Nitric oxide conversion was calculated by dividing the moles of NO_2 in the products by the moles of NO fed. No N_2 was observed to be formed. Catalytic activities are reported as turnover frequency (*TOF*) based on surface sites counted by oxygen chemisorption (eqn. 1) and HCHO productivity (eqn. 2):

$$TOF \ [s^{-1}] = \frac{CH_4 \ \text{flowrate} \ [\mu mol/s] \times X_{CH_4}}{\text{Catalyst weight} \ [g] \times \text{Quantity of sites} \ [\mu mol/g]} \tag{1}$$

$$Productivity \ [s^{-1}] = \frac{CH_4 \ flowrate \ [\mu mo \ / \ ] \times X_{CH_4} \times HCHO \ selectivity}{Catalyst \ weight \ [g]} \tag{2}$$

Contact-time measurements on VO_x/SiO_2 and MnO_x/SiO_2 were carried out by varying the total flow rates (68 - 210 μmol s^{-1}) while keeping the reactant gas ratio constant. The total pressure was 0.10 MPa, the temperature was 400 °C, and the bed volume was 1.3 cm^3. The contact time was calculated by:

$$\text{Contact time} \ [s] = \frac{\text{Quantity of sites} \ [\mu mol/g] \times \text{Catalyst weight} \ [g]}{CH_4 \ \text{flowrate} \ [\mu mol/s]} \tag{3}$$

Measurements were taken at increasing and then decreasing contact time to be certain the catalyst was not deactivating during the course of the measurements.

2.6.   In situ infrared spectroscopy

Infrared spectroscopic measurements of VO_x/SiO_2 and MnO_x/SiO_2 were collected in situ using a Fourier transform infrared spectrometer (JASCO FT/IR-610) equipped with an MCT detector. The samples, in the form of self-supporting wafers of diameter 1.0 cm (ca. 11 mg), were placed at the center of an infrared flow cell equipped with KBr windows which were maintained at 25 °C by a circulation cooler. To minimize gas-phase interference and reduce dead volume inside the cell, KBr rods were placed in the free space inside the reactor. Before measuring the spectra, the samples were pretreated in flowing 20% O_2/He (34 µmol s^{-1}) at 500 °C for 1 h and then cooled to 400 °C in a He flow (34 µmol s^{-1}). The spectra were recorded at 400 °C in the absorbance mode by accumulating 100 scans with a resolution of 4 cm^{-1} and in the region of 4000 - 1000 cm^{-1}. The experiments involved three parts. The first consisted of flowing a mixture of 1% NO, 1% O_2 and 98% He (68 µmol s^{-1}) over the catalyst with continuous monitoring of NO_x species formation until saturation was achieved. The samples were then purged with He to remove gaseous and weakly adsorbed species before subsequently injecting 10% CH_4 in He (68 µmol s^{-1}) and monitoring adsorbed species until no changes were observed in the spectra. The last step consisted of flowing a reaction gas mixture of 10% CH_4, 1% NO, 1% O_2 and 88% He (68 µmol s^{-1}) and monitoring surface intermediates at reaction conditions.

3.   Results and discussion

3.1.   Catalyst characterization

Table 1 shows BET surface areas, nominal metal oxide loadings, and calculated surface densities. The metal loadings corresponded to the same moles of metal (0.10 mmol g^{-1}) in each

sample. The surface densities are the number of metal atoms per unit surface area of the catalyst (MO_x atoms nm^{-2}):

$$MO_x \text{ surface density } = \frac{f_{oxide} \times 6.02 \times 10^{23}}{S_{BET} \times MW_{oxide} \times 10^{18}} \tag{4}$$

In this equation, f_{oxide} is the fractional loading of the metal oxide (using the phases in parenthesis in column 2 of Table 1 as the basis), S_{BET} is the BET surface area of the catalyst (m^2 g^{-1}) before reaction, MW_{oxide} is the molecular weight of the oxide (g mol^{-1}), and 10^{18} is a conversion factor to convert m^2 to nm^2. The surface densities were similar (~0.2 atoms nm^{-2}) and below reported monolayer surface coverages (< 2 atoms nm^{-2}) of these oxides on silica [35,39,40].

Table 1. Metal oxide loading, BET surface area and MO_x surface density of supported catalysts.

Catalyst	Metal oxide loading / wt%	BET surface area (S_{BET}) / m^2 g^{-1}	MO_x surface density / atoms nm^{-1}
VO_x/SiO_2	0.9 (V_2O_5)	362	0.17
CrO_x/SiO_2	0.8 (Cr_2O_3)	353	0.18
MnO_x/SiO_2	0.9 (MnO_2)	313	0.20
NbO_x/SiO_2	1.4 (Nb_2O_5)	348	0.18
MoO_x/SiO_2	1.5 (MoO_3)	314	0.20
WO_x/SiO_2	2.4 (WO_3)	328	0.19

Fig. S1 shows the XRD patterns of the catalysts and it can be seen that crystalline metal oxide phases were not detected for any of the catalysts, with the XRD patterns resembling that of the pure SiO_2 support. These results are similar to those reported previously for SiO_2-supported samples with low MO_x surface densities (< 2 atoms of MO_x per nm^2) [34,39,40], suggesting that the supported oxides were highly dispersed.

Fig. 1 shows the H_2O (m/z = 18) TPR traces for the supported metal oxides. The experiments were performed to determine the onset of reduction (T_{red}) of each catalyst, which is indicated by an arrow and corresponds to the lowest temperature at which the mass signal

increased sharply. Previous studies have indicated that surface reduction principally takes place at this temperature [34,35,40]. Fig. 1 shows that T_{red} increased in the order: MnO_x/SiO_2 (225 °C) < CrO_x/SiO_2 (320 °C) < VO_x/SiO_2 (369 °C) < MoO_x/SiO_2 (412 °C) < WO_x/SiO_2 (511 °C) < NbO_x/SiO_2 (588 °C). The trend showed a decrease in T_{red} moving across the periodic table but an increase in T_{red} moving down. These temperatures were used for oxygen chemisorption measurements. The peaks in each trace at temperatures below 600 °C correspond to bulk reduction of the oxides, with multiple peaks being attributed to sequential reduction. Features above 600 °C likely include contributions from dehydroxylation [40]. All the features above 400 °C are irrelevant to the work here as they occur above the temperature range for catalyst testing.
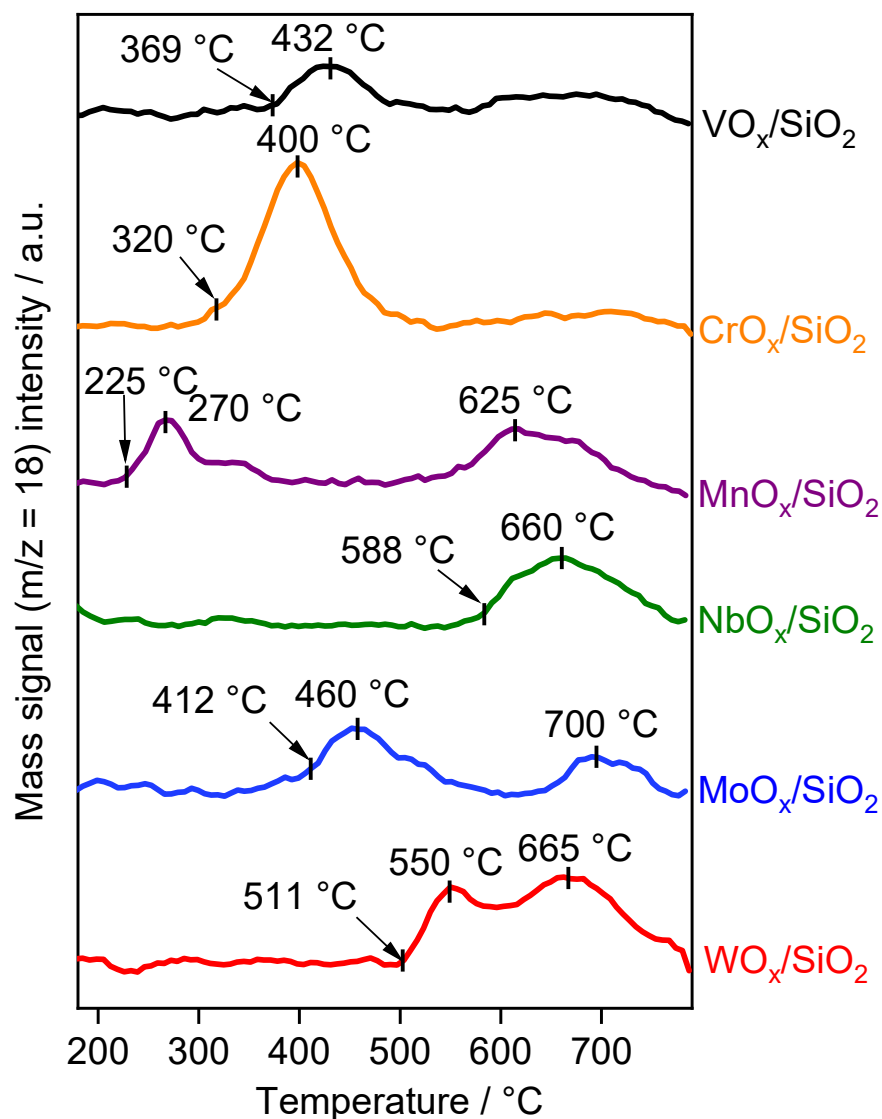
Fig. 1. TPR traces (m/z = 18) for silica-supported metal oxides.

Table 2 lists the molecular oxygen uptakes and dispersions for the catalysts. The uptakes were measured at T_{red} after pretreatment of the samples at 500 °C for 1 h in flowing 20% O_2/He, followed by reduction at T_{red} for 2 h in flowing H_2. This procedure has been shown to give a reasonable estimate of the number of surface sites on a variety of supported metal oxides [34,35, 40]. The uptakes (24 - 66 μmol g^{-1}) were used to calculate dispersion by correcting for

adsorption on the SiO$_2$ support and by assuming a stoichiometry of one oxygen atom per surface

metal atom. Using V$_2$O$_5$, Cr$_2$O$_3$, MnO$_2$, Nb$_2$O$_5$, MoO$_3$, and WO$_3$ as bases, the dispersion was

calculated using the measured O$_2$ uptakes of VO$_x$/SiO$_2$, CrO$_x$/SiO$_2$, and NbO$_x$/SiO$_2$, and twice

the O$_2$ uptakes of MnO$_x$/SiO$_2$, MoO$_x$/SiO$_2$, and WO$_x$/SiO$_2$. The dispersion ranged from low

(21%) to high (100%); except for VO$_x$/SiO$_2$, the results suggest the presence of surface oxides,

which were too dispersed to be visible by XRD.

Table 2. Oxygen uptake on the supported metal oxides.

Catalyst	$T_{red} = T_{ads}$[a] / °C	O$_2$ uptake / μmol g^{-1}	Dispersion / %
SiO$_2$[b]	-	13	-
VO$_x$/SiO$_2$	369	66	100
CrO$_x$/SiO$_2$	320	57	84
MnO$_x$/SiO$_2$	225	36	45
NbO$_x$/SiO$_2$	588	24	21
MoO$_x$/SiO$_2$	412	48	67
WO$_x$/SiO$_2$	511	46	64

[a]$T_{red} = T_{ads}$ (temperature used for reduction and O$_2$ chemisorption measurements)
[b]Results from 225 °C, 369 °C and 588 °C were averaged

3.2.   Raman spectroscopic characterization

Raman spectroscopy was used to aid in determining the degree of metal oxide dispersion

on the silica surface. Fig. 2 shows Raman spectra of the samples recorded in air at 30 °C under

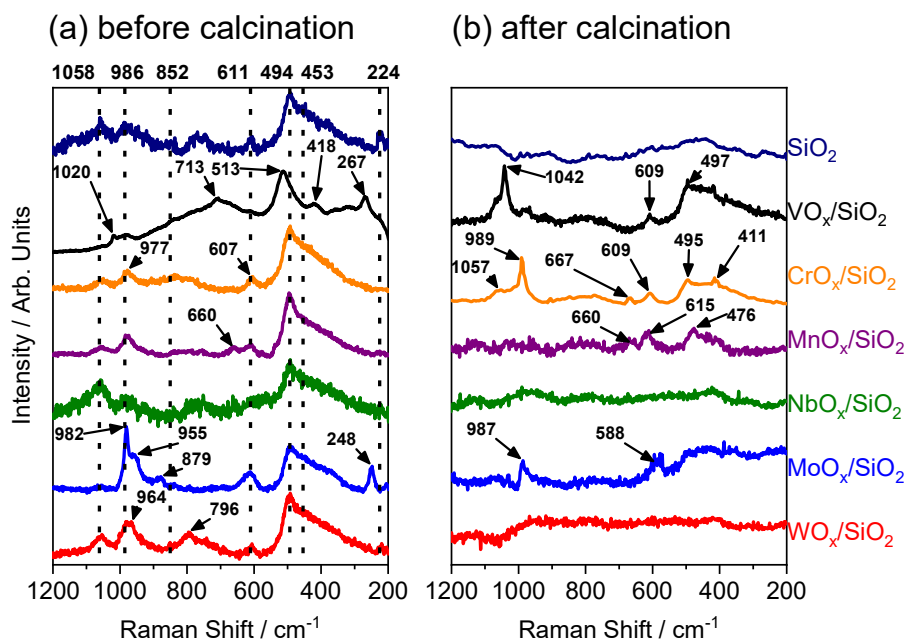N$_2$ after dehydration at 500 °C.

Fig. 2. Raman spectra (λ=488 nm) of the silica-supported metal oxides (a) before and (b) after dehydration.

The Raman spectrum of the SiO_2 support shows a series of distinct bands, marked with dotted vertical lines in Fig. 2a, which are typical of hydrated silica [41]. The band at 986 cm^{-1}, which is associated with surface silanol groups, overlaps M=O stretching vibrations assigned to several surface metal oxide species [41]. Although this band is not present in the Raman spectra after dehydration, the silica sample became highly luminescent, leading to lower spectral quality. Nonetheless, comparison between Raman spectra of the MO_x/SiO_2 catalysts and support are informative about the nature of the surface metal oxide species.

The hydrated VO_x/SiO_2 sample shows a band at 1020 cm^{-1} which overlaps the silanol band. After dehydration the vanadium modified catalyst showed far less luminescence than the silica support, allowing identification of highly dispersed vanadium oxide units on the surface. A band at 1042 cm^{-1} is observed for VO_x/SiO_2, which is consistent with previous reports of silica

14

with low vanadium loadings [35,41,42,43,44,45,46] corresponding to a vanadyl group (V=O) with three bridging siloxy links to the surface. Bands for crystalline V_2O_5 were not observed [41].

The hydrated CrO_x/SiO_2 sample shows a shoulder at 977 cm^{-1} which overlaps the silanol band. The Raman spectrum of the dehydrated CrO_x/SiO_2 sample shows a band at 989 cm^{-1} which is associated with monomeric CrO_x species [47, 48, 49]. No bands associated with α-Cr_2O_3 are observed, which would be expected with higher Cr loadings [47].

Before dehydration the MnO_x/SiO_2 sample shows a band at 660 cm^{-1} that may indicate MnO_x clusters on the surface [50,51]. A second band around 615 cm^{-1} is expected but cannot be distinguished from the silica support band at 611 cm^{-1}. After dehydration MnO_x/SiO_2 shows a distinct Raman feature at 615 cm^{-1} which is assigned to a Mn-O-Si bond vibration [52]. The 660 cm^{-1} band become very weak after dehydration. The assignment is therefore somewhat ambiguous. Nonetheless, bands associated with bulk crystalline manganese oxides are not present [52].

Raman spectra of the hydrated NbO_x/SiO_2 sample appear nearly identical to those of the bare SiO_2 support. Notably, no Nb_2O_5 bands are observed [41]. The NbO_x/SiO_2 sample was highly luminescent after dehydration. Given that no SiO_2 bands could be observed under these conditions, it is unsurprising that bands associated with surface NbO_x species could not be observed. These would be expected at about 980 cm^{-1} [53].

Before dehydration the MoO_x/SiO_2 sample shows a strong peak at 982 cm^{-1} overlapping the silanol. After dehydration the band shifts to 987 cm^{-1} and weakens. These bands are typical of monomeric molybdenum oxide species [43]. A higher frequency band is expected at higher

loadings where oligomeric species are formed on the surface [43,54,55]. No bands related to crystalline MoO_3 are observed under either set of conditions [41].

The Raman spectra of the hydrated WO_x/SiO_2 sample showed a shoulder at 964 cm^{-1} and a weak band at 796 cm^{-1} which could be indicative of highly dispersed WO_x species [56]. After dehydration the sample was highly luminescent. The band expected for highly dispersed dehydrated WO_x around 980 cm^{-1} was not observed. Bands associated with crystalline WO_3 were not observed [41,56]. Overall, the characterization by laser Raman spectroscopy gives evidence for the presence of highly dispersed oxidic species on the silica surface.

3.3.   Catalyst activity

Methane oxidation was studied at ambient pressure between 300 and 400 °C on the silica-supported metal oxide catalysts. Table 3 summarizes the activity at 400 °C for each catalyst using either O_2 or $NO+O_2$ as the oxidant. The CH_4 conversions were generally very low because of the use of low concentrations of oxidants; a CH_4/O_2 ratio of 20/1 means the maximum conversion is 2.5% if CO_2 is the only product. Notably, when O_2 alone was used as the oxidant only MnO_x/SiO_2 showed conversion. Blank measurements with the SiO_2 support gave negligible activity.

Table 3 also lists M=O Raman vibrational frequencies for dehydrated samples. Although limited values are available, there is no correlation of these with reactivity as pointed out by Haber for methanol oxidation [1].   Fig. 3 shows the CH_4 conversion and HCHO selectivity as a function of temperature for each of the supported metal oxides using an $NO+O_2$ mixture as the oxidant. All measurements of reactivity were done by raising and then lowering the temperature and the obtention of smooth curves indicates that there was no deactivation during the

16

experiments. Methane conversion on MnO_x/SiO_2 was the highest, followed by that on

VO_x/SiO_2, and then on CrO_x/SiO_2 (Fig. 3a).

Table 3. Reactivity in methane oxidation at 400 °C.

Samples	Oxidant	CH_4 conv. / %	Selectivity / %		Turnover rates / $\times 10^{-3}$ s^{-1}	HCHO Productivity μmol g_{cat}^{-1} h^{-1}	M=O bond vibration frequency[a] cm^{-1}
			HCHO	CO_2			
VO_x/SiO_2	NO/O_2	0.28	33	67	1.2	91	1042
	O_2	<0.001	-	-	-	-	
CrO_x/SiO_2	NO/O_2	0.18	0	100	0.9	0	989
	O_2	<0.001	-	-	-	-	
MnO_x/SiO_2	NO/O_2	0.74	0	100	2.8	0	—
	O_2	0.24	0	100	0.9	0	
NbO_x/SiO_2	NO/O_2	0.11	0	100	0.5	0	—
	O_2	<0.001	-	-	-	-	
MoO_x/SiO_2	NO/O_2	0.045	86	14	0.1	38	988
	O_2	<0.001	-	-	-	-	
WO_x/SiO_2	NO/O_2	0.045	72	28	0.1	31	—
	O_2	<0.001	-	-	-	-	

Conditions: CH_4 (20 kPa), NO (1 kPa) and O_2 (1 kPa), balanced by He and Ar at a total flow rate of 68 μmol s^{-1}

[a] Conditions: N_2, 30 °C, 488 nm laser, dehydrated at 500 °C.

The conversions on NbO_x/SiO_2, MoO_x/SiO_2 and WO_x/SiO_2 were all similar and only

detectable above 350 °C. During the reactions, CO_2 and HCHO were the only carbon-containing

products observed. The CrO_x/SiO_2, MnO_x/SiO_2 and NbO_x/SiO_2 catalysts gave only CO_2, whereas

the VO_x/SiO_2, MoO_x/SiO_2 and WO_x/SiO_2 samples produced both CO_2 and HCHO (Fig. 3b). The

results are consistent with the known catalytic chemistry of these samples: the oxides of

chromium, manganese, and niobium favor total oxidation, whereas the oxides of vanadium,

molybdenum and tungsten promote partial oxidation [57,58,59]. The HCHO selectivity

decreased with increasing temperature, likely because of overoxidation. Past work by Haber

[11] associated total oxidation with electrophilic oxygen (O_2^{2-}, O_2^-, O^-) and partial oxidation with

nucleophilic oxygen (O^{2-}), and this may apply here.
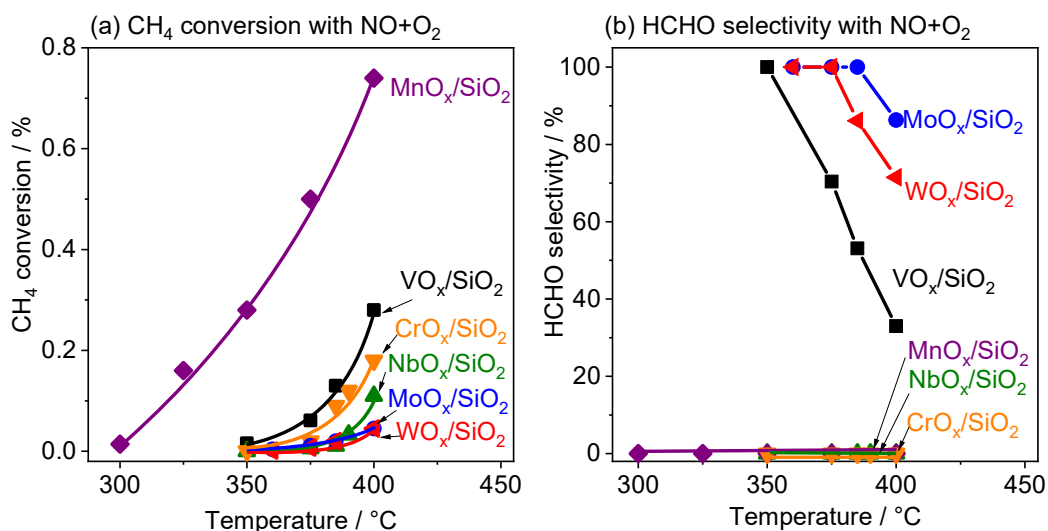
Fig. 3. Comparison of (a) methane conversion and (b) HCHO selectivity of the supported metal oxide catalysts using $NO+O_2$ mixture as the oxidant ($CH_4:NO:O_2:inert = 20:1:1:78$) at 0.1 MPa and 6000 L kg^{-1} h^{-1} space velocity.

Fig. 4 shows CH_4 conversion and HCHO selectivity versus temperature using only O_2 as

the oxidant. In this case, only MnO_x/SiO_2 showed detectable conversion and only CO_2 was

formed. The results indicate that dissociation of molecular oxygen does not proceed easily on

these samples at the conditions of this study, and NO addition was important for the increase in

methane reactivity. This is in general agreement with findings by Fierro and coworkers on

V_2O_5/SiO_2 [25,26,60], although in those studies NO was suggested to have acted as a radical initiator for gas-phase reactions prevalent at high temperatures (> 600 °C). In the present study gas-phase methane reactions were not detected due to the milder conditions used, indicating that NO played a different role to that observed by Fierro and coworkers. Instead, NO reacted with O_2 in the gas phase to form NO_2, which was then able to oxidize CH_4.
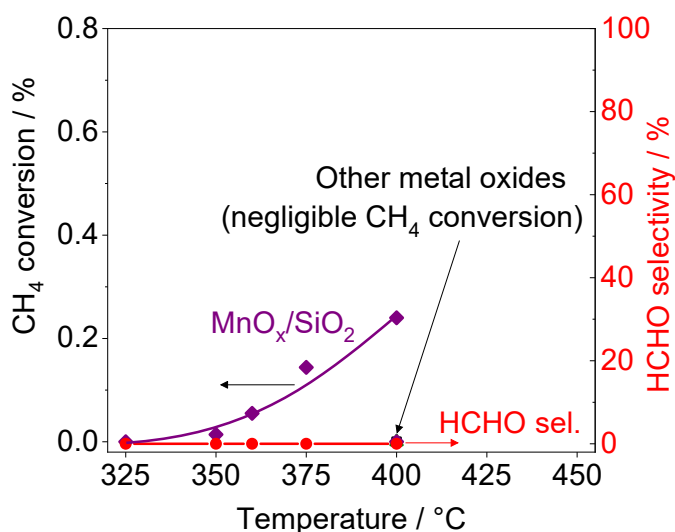

Fig. 4. Comparison of methane conversion and HCHO selectivity of the supported metal oxide catalysts using O_2 as the oxidant (CH_4:O_2:inert = 20:1:79) at 0.1 MPa and 6000 L kg^{-1} h^{-1} space velocity.

Fig. 5 shows the conversions of O_2 and NO, and the selectivities of NO to NO_2 and N_2 as a function of temperature during the oxidation of methane on VO_x/SiO_2 (Fig. 5a) and MnO_x/SiO_2 (Fig. 5b) for the same conditions as Fig. 3. Data for CrO_x/SiO_2, NbO_x/SiO_2, MoO_x/SiO_2 and WO_x/SiO_2 can be found in Fig. S2 (SI). The total oxygen conversion (✱) on any catalyst did not change appreciably within the entire temperature range. This is because O_2 conversion to NO_2 (✚) was offset by O_2 conversion to carbon-containing products and water (✕). The total O_2 conversion hovered around 50% because nearly half of the initial amount of O_2 fed was used for

the stoichiometric gas-phase NO oxidation reaction to form NO_2 ($NO + \frac{1}{2} O_2 \rightarrow NO_2$) [61,62]. The NO conversion (★) decreased with increasing temperature because the NO to NO_2 reaction is disfavored thermodynamically [32] and because a fraction of NO_2 is consumed in the methane oxidation reaction.

During the reaction, the involvement of NO_2 in functionalizing methane is evidenced by the differences between the results of VO_x/SiO_2 and MnO_x/SiO_2. The NO conversion and O_2 conversion to carbon-containing products and H_2O changed more appreciably over MnO_x/SiO_2 as temperature increased, consistent with the increase in methane conversion. For both catalysts NO_2 was the only nitrogen-containing product formed from the NO reaction, indicating that reduction to N_2 did not occur at any temperature on any catalyst (Fig. 5 and Fig. S2). Furthermore, full mass balances in nitrogen and oxygen were achieved. Collectively, these results indicate a $2NO + O_2 \rightleftharpoons 2NO_2$ cycle, which permitted the dissociation of O_2 at moderate conditions. This is the reason for the higher methane reactivity using the $NO+O_2$ mixture compared to O_2. The $2NO + O_2 \rightleftharpoons 2NO_2$ reaction occurs readily in the gas-phase as demonstrated kinetically and thermodynamically [32].

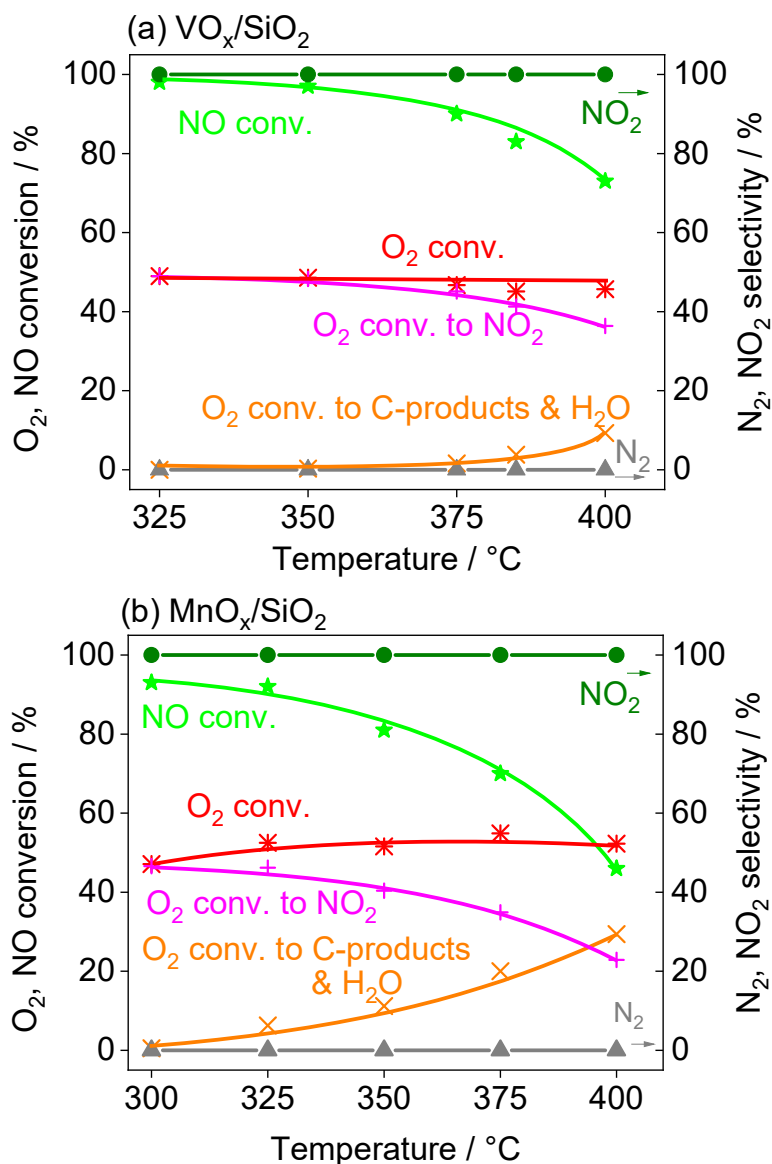Fig. 5. Oxygen and NO conversion on (a) VO_x/SiO_2 and (b) MnO_x/SiO_2 using $NO+O_2$ mixture as the oxidant ($CH_4:NO:O_2:inert = 20:1:1:78$) at 0.1 MPa and 6000 L kg^{-1} h^{-1} space velocity.

Fig. 6 shows the turnover frequencies and HCHO production rates as a function of temperature on the metal oxide catalysts using the $NO+O_2$ mixture. The rates were calculated with the use of the surface metal atoms from the high temperature oxygen chemisorption experiments. The total turnover rates follow the same trend as the CH_4 conversion: $MnO_x/SiO_2 >$

$VO_x/SiO_2 > CrO_x/SiO_2 > NbO_x/SiO_2 > MoO_x/SiO_2 \approx WO_x/SiO_2$ (Fig. 6a). However, the trend cannot be explained by differences in reducibility since it does not track with the order of the peak reduction temperature of the oxides. This may be because the oxide-support interaction was not primarily responsible for methane activation, or perhaps that reactivity was dependent on the activation of both methane and oxygen. The trend appears to follow the positions in the periodic table of the transition metal element: elements in the first row and to the right in the periodic table were most active. Also, as will be shown in the next section, the difference in reactivity could be related to reactivity of surface nitrate species. Fig. 6b shows that the HCHO production rates follow the order $VO_x/SiO_2 > MoO_x/SiO_2 \approx WO_x/SiO_2$. As noted previously, only redox active oxides produced HCHO, which may mean that lattice oxygen is participating in the reaction. Since the catalysts here are surface dispersed oxide species, lattice oxygen here is used to denote oxygen that is not adsorbed, and includes oxygen associated with those oxides and oxygen forming linkages to the support. The involvement of lattice oxygen in the oxidation of methane has been confirmed by others from isotopic studies [16,63,64]; however, the manner of participation may be different with the $NO+O_2$ mixture. Because methane oxidation with only O_2 on VO_x/SiO_2, MoO_x/SiO_2, and WO_x/SiO_2 was negligible, it can be concluded that the lattice oxygen had negligible reactivity at $\leq 400\ °C$. Thus, it is reasoned that lattice oxygen may have been involved in the formation of surface nitrate species which subsequently oxidized methane, as will be discussed in the next section.
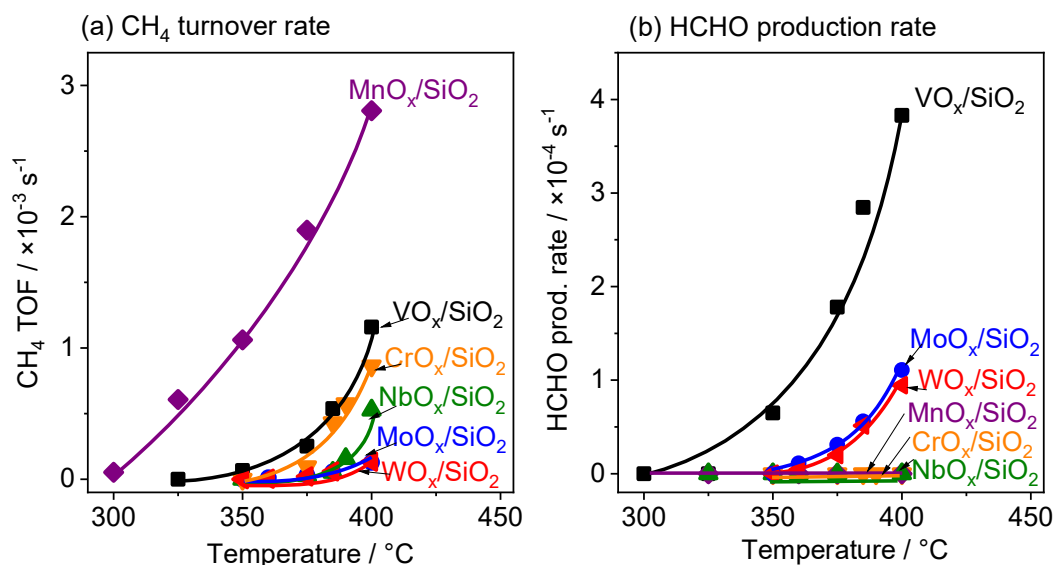
Fig. 6. Comparison of (a) turnover frequencies and (b) HCHO production rates for methane oxidation over the supported metal oxides using $NO+O_2$ mixture as the oxidant ($CH_4:NO:O_2:inert = 20:1:1:78$) at 0.1 MPa and 6000 L kg^{-1} h^{-1} space velocity.

Reaction sequences may be obtained from contact time measurements [65,66]. Such studies of methane oxidation on MnO_x/SiO_2 and VO_x/SiO_2 were carried out at 400 °C using the $NO+O_2$ mixture as the oxidant. The MnO_x/SiO_2 catalyst was chosen because it exhibited the highest total turnover rate but produced only CO_2 and H_2O, whereas the VO_x/SiO_2 catalyst was chosen because it displayed the highest HCHO production rate. Fig. 7 shows HCHO and CO_2 selectivities and CH_4 conversions versus contact time on VO_x/SiO_2 (Fig. 7a) and MnO_x/SiO_2 (Fig. 7b). As expected, the CH_4 conversion increased with increasing contact time on both catalysts; however, the product selectivities differed. VO_x/SiO_2 formed HCHO and CO_2, with the selectivity to HCHO decreasing from 100% to 36% as contact time increased. In contrast, MnO_x/SiO_2 produced only CO_2 over the entire range of measurement, which indicates that Mn oxide possesses an inherent deep oxidation activity. Based on these results, reaction schemes for the oxidation of methane with the $NO+O_2$ mixture were proposed: (1) VO_x/SiO_2: $CH_4 \rightarrow$ HCHO

23

$\rightarrow CO_2$; and (2) MnO_x/SiO_2: $CH_4 \rightarrow CO_2$. It is important to note that these sequences are empirical because the formation of methanol as a primary product cannot be ruled out unambiguously due to its high reactivity under these conditions.
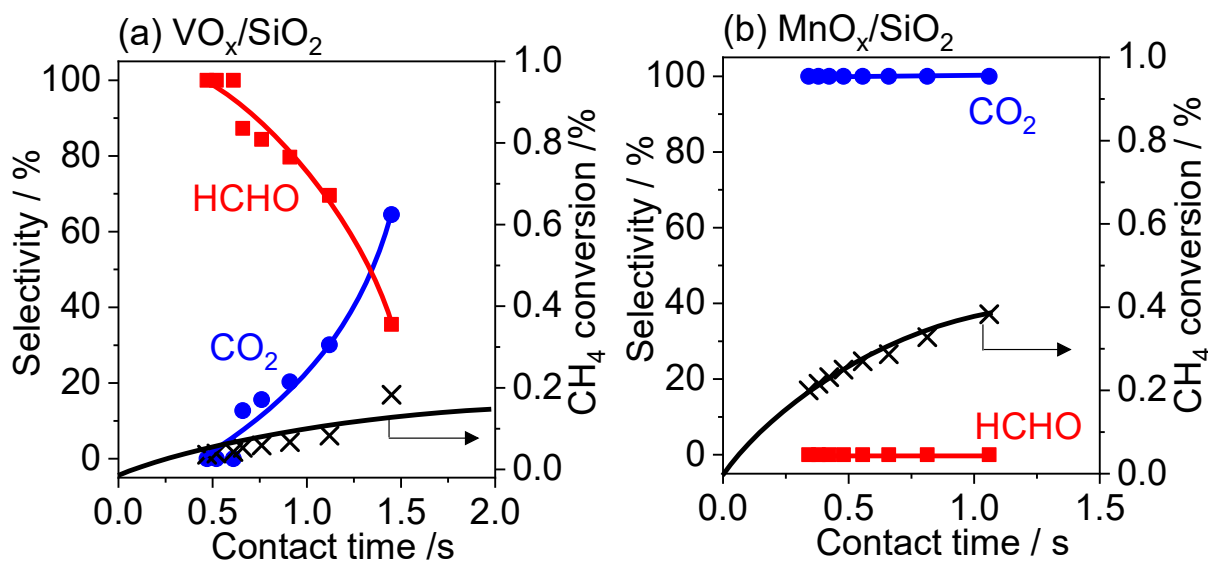

Fig. 7. Effect of contact time for the methane oxidation on (a) VO_x/SiO_2 and (b) MnO_x/SiO_2 using $NO+O_2$ mixture (CH_4:NO:O_2:inert = 20:1:1:78) at 400 °C and 0.1 MPa.

A substantial amount of work has been reported on the oxidation of methane by a variety of solid catalysts and oxidants, and the topic has been reviewed recently [67,68]. The catalysts include vanadium oxide, molybdenum oxide, and metal-exchanged zeolites, and the oxidants include O_2, N_2O and H_2O_2. The studies with O_2 were conducted often at high temperature (> 550 °C) and continuous conditions [20,69], those with N_2O were performed typically at moderate to high temperature (300 - 600 °C) and also continuous conditions [70,71] or at low temperatures (< 300 °C) using a stepwise operation [72,73], and those with H_2O_2 were carried out mostly at low temperatures (<100 °C) in the liquid phase [74,75]. Unfortunately, the

substantial differences in conditions make direct comparisons difficult, and only a few investigations were conducted at the conditions of this study. For the relevant studies, the results are compared to the present work based on turnover frequency (TOF, mol mol_{surf}^{-1} s^{-1} or simplified as s^{-1}). This is because the TOF represents the most fundamental comparison of intrinsic partial oxidation activity. The comparisons are shown in Table S2. The TOF over VO_x/SiO_2 (3.8×10^{-4} s^{-1}), MoO_x/SiO_2 (1.1×10^{-4} s^{-1}), and WO_x/SiO_2 (9×10^{-5} s^{-1}) in this work compares favorably to literature reports on Fe-ZSM-5 (5.6×10^{-5} s^{-1}) [76], Fe/Ferrierite (7.0×10^{-5} s^{-1}) [77], $FePO_4$ (4.5×10^{-3} s^{-1}) [70], $FePO_4$/MCM-41 (8.7×10^{-5} s^{-1}) [70], and H-Cu-SSZ-13 (3.2×10^{-5} s^{-1}) [78] using N_2O, and FeCu/ZSM-5 (3.9×10^{-6} s^{-1}) [79] using H_2O_2. In contrast, the TOF was one to two orders of magnitude lower than that on $FePO_4$ using O_2 [80] and N_2O [70,80] and was substantially lower than on Li/MgO using O_3 [81]. These latter studies were either conducted in the explosive regime [80] or with high concentrations of expensive oxidant [70], or were aided by substantial contributions from gas-phase reactions [81]. Hence, the results from the present work are promising, particularly because they were achieved with O_2 as the ultimate oxidant, whereas the rates from the cited works were obtained with activated oxidants. This is consistent with results from our recent work on Pt/Y_2O_3 [30, 31].

3.4.   In situ Fourier transform infrared spectroscopy (FTIR) analysis

Infrared spectra of the VO_x/SiO_2 and MnO_x/SiO_2 samples were obtained in situ during exposure to various gases at 400 °C in order to characterize adsorbed species and explain differences in reactivity. As with the contact time measurements, these two samples were selected as representative catalysts for deep oxidation (MnO_x/SiO_2) and partial oxidation (VO_x/SiO_2). The experimental sequence consisted of dosing the catalysts with a gas mixture (1%

NO and 1% O_2 in He) until saturation occurred, purging with He, introducing 10% CH_4 in He for 30 min, purging with He, feeding a reaction gas mixture (10% CH_4, 1% NO, 1% O_2 in He), and purging with He. These steps allowed the study of adsorbed NO_x species and their reactivity, as well as the study of surface intermediates at reaction conditions. All spectra are shown here with subtraction of the catalyst background.

Fig. 8 shows a series of spectra during NO+O_2 adsorption on the VO_x/SiO_2 (a) and MnO_x/SiO_2 (b) catalysts as a function of time. The spectra were similar, with bands appearing after about 10 min of exposure: a weak doublet at 1630 and 1602 cm^{-1} and a more intense doublet at lower wavenumbers that reached maximum intensity after ca. 25 min. The weak doublet can be assigned to NO_2 adsorbed on SiO_2, which has been observed on a wide variety of systems, according to a comprehensive review by Hadjiivanov and coworkers [82]. The more intense doublet is likely associated with the metal oxides and the silica, although unambiguous assignment is complicated by a combination of scant infrared data for silica-supported metal oxides and large disagreements in the assignments of the available literature data for other systems [82]. The doublet is probably due to ionic NO_x nitrate species (NO_3^-) since they are considered to be the most stable species formed after NO+O_2 co-adsorption on various oxides [82]. According to previous studies, surface nitrates are formed via the replacement of a monovalent surface anion by NO_3^-, through the oxidation of a surface cation ($M^{n+} + NO_2 + 1/2\,O_2 \rightarrow M^{(n+1)+}$-$NO_3^-$ or $M^{n+} + NO + O_2 \rightarrow M^{(n+1)+}$-$NO_3^-$), or via the oxidation of adsorbed nitrites by reactive oxygen species as follows ($NO_2^- + O^{2-} \rightarrow NO_3^- + 2e^-$) [82,83,84,85,86]. Thus, it is suggested that the lower wavenumber peaks of the doublets (1389 and 1363 cm^{-1} for VO_x/SiO_2) and (1399 and 1356 cm^{-1} for MnO_x/SiO_2) corresponds to monodentate nitrates formed by adsorption of NO_2 on the supported metal oxide and the higher wavenumber peak of the doublets

26

(1389 cm^{-1} for VO$_x$/SiO$_2$ and 1399 cm^{-1} for MnO$_x$/SiO$_2$) is due to monodentate nitrates formed on the bridging oxygen between the metal oxide and silica (M-O-Si). The adsorption of NO$_2$ is weak on SiO$_2$ and results in bands at 1686 and 1745 cm^{-1}, which disappear after evacuation [87].
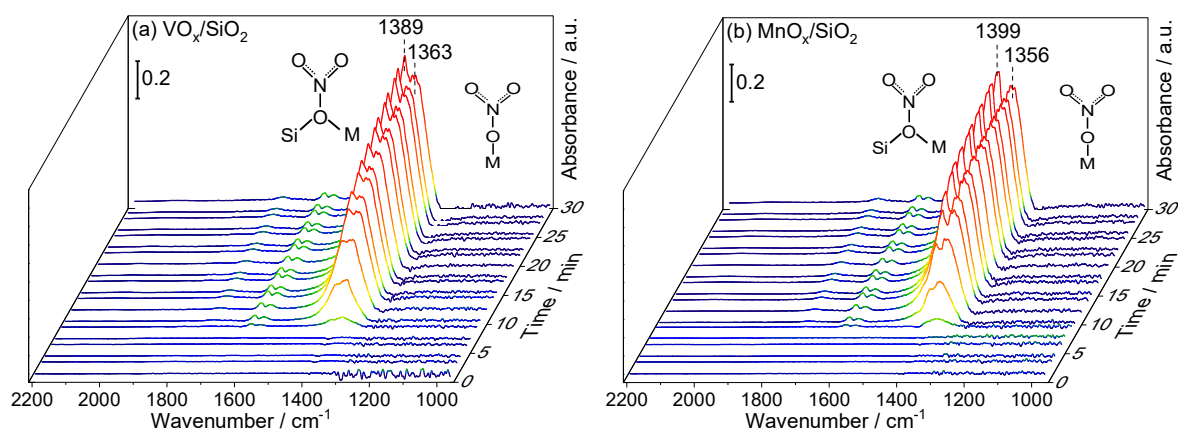

Fig. 8. In situ FTIR spectroscopy results for NO+O$_2$ adsorption on (a) VO$_x$/SiO$_2$ and (b) MnO$_x$/SiO$_2$ with increase in time. Conditions: Flow of NO+O$_2$ (NO:O$_2$:He = 1:1:98, 68 μmol s^{-1}) at 400 °C.

Fig. 9 shows adsorbed NO$_x$ species on (a) VO$_x$/SiO$_2$ and (b) MnO$_x$/SiO$_2$ at various conditions. The sequence of measurements is from bottom to top, starting with (1) spectra taken in He of adsorbed species after NO+O$_2$ exposure, followed by (2) spectra after CH$_4$ introduction, then (3) spectra in He after the CH$_4$ exposure, then (4) spectra during CH$_4$, NO, and O$_2$ reaction, and finally (5) spectra in He after the reaction. Fig. S3 shows the same figure at an extended scale. It is not possible to see bands corresponding to M-O and M-O$_2$ bonds, which would have appeared at wavenumbers below the cutoff region for oxides due to self-absorption [87]. The weak doublet due to adsorbed NO$_2$ on SiO$_2$ is not visible on the spectra taken in He, consistent with findings that the bands disappear easily after evacuation or purging with inert gas [82]. In contrast, the doublet for the monodentate nitrate species can be observed on both catalysts at all

conditions, although with some notable differences in peak intensities depending on the atmosphere.

The reaction of monodentate nitrate species on the metal oxides with CH_4 is evident from the appreciable decrease of the areas upon the introduction of CH_4 (Nos. 1 and 2). The decrease was more pronounced on MnO_x/SiO_2, consistent with the higher reactivity of methane discussed earlier. There was little change with He (No. 3). However, there was an increase in the areas of the nitrates during the flow of 10% CH_4, 1% NO and 1% O_2 in He (No. 4), likely due to contributions from weakly adsorbed species. The lack of measurable consumption of the nitrates even in the presence of CH_4 in this step reflects the low reactivity in the methane reaction. Recall from Table 3 that CH_4 conversion on these catalysts was low (0.28% on VO_x/SiO_2 and 0.74% on MnO_x/SiO_2 at 400 °C). The areas were restored after reintroduction of the $NO+O_2$ mixture and purging with He (No. 5), confirming the consumption of the nitrates during the CH_4 exposure.

To better quantify the changes, the doublet bands were deconvoluted and are shown in Fig. S4 with the integrated areas reported in Table S3. For the MnO_2/SiO_2 catalyst the deconvoluted spectra show that for the 1399 cm^{-1} high wavenumber peak there is a substantial decrease in the integrated area in going from (1) NO_x in He to (2) NO_x in CH_4 (decrease in area is 83%), indicating that the NO_2 associated with that wavenumber is being consumed by reaction with CH_4. For the 1356 cm^{-1} low wavenumber peak there is a much smaller decrease in the integrated area (decrease is 20%). For the VO_x/SiO_2 catalyst the corresponding decreases in area of the 1389 cm^{-1} high wavenumber peak and the 1363 cm^{-1} wavenumber peak are respectively 14% and 13%, so there appears to be no preferential use of either NO_2 species in partial oxidation. It is important to state that during the CH_4 exposure only the vibrational band due to

gas-phase CH_4 was observed at 3010 cm^{-1} (Fig. S3); no peaks due to methyl or methoxy groups were observed in the C-H region. This suggests that these species were highly reactive under the $NO+O_2$ mixture, in agreement with our previous studies [30,31].
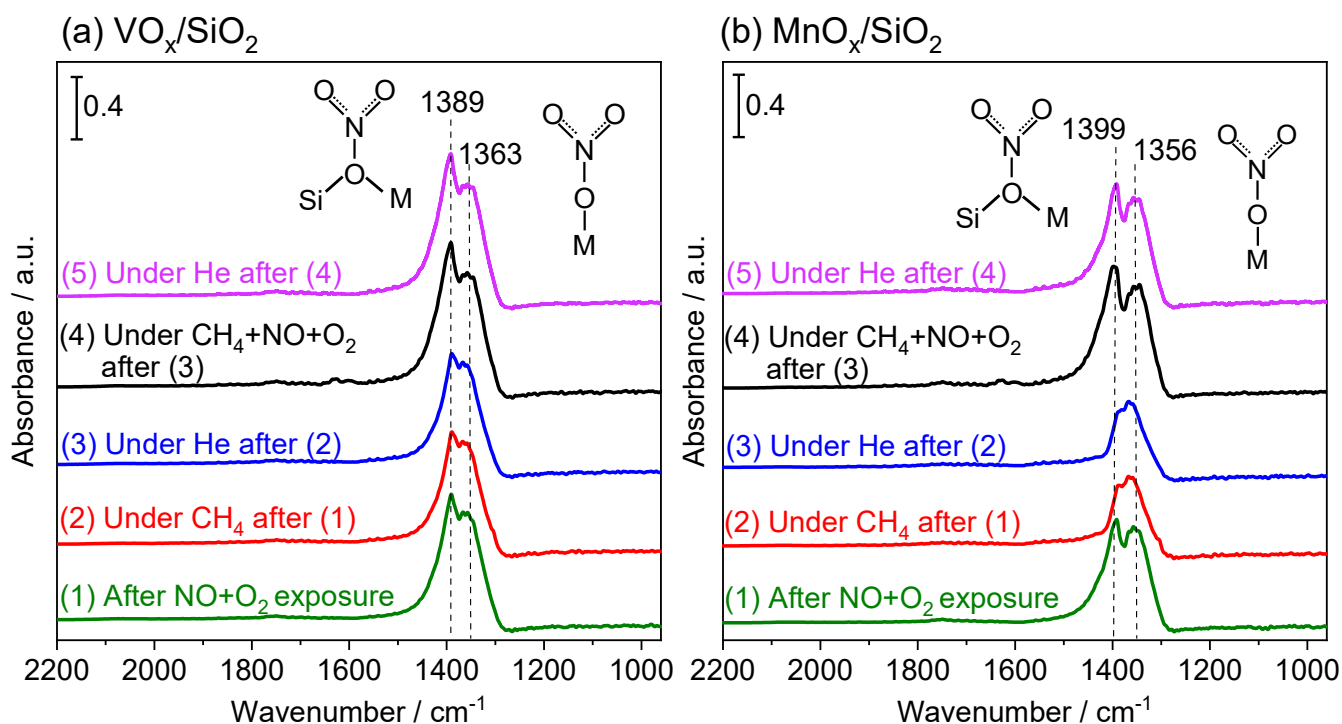

Fig. 9. In situ FTIR spectroscopy results for the reaction of adsorbed NO_x species on (a) VO_x/SiO_2 and (b) MnO_x/SiO_2 with CH_4 at 400 °C. Conditions: (1) under He after flow of $NO:O_2:He = 1:1:98$ (68 μmol s^{-1}), (2) under flow of 10% CH_4 in He (34 μmol s^{-1}) for 30 min, (3) under He after flow of CH_4, (4) under flow of $CH_4:NO:O_2:He = 10:1:1:88$ (68 μmol s^{-1}) for 30 min, and (5) under He after the CH_4+NO+O_2+He reaction.

On the basis of the results in this study and previous information on the mode of adsorbate bonding in oxidation reactions [88, 89], a reaction scheme is proposed for the selective oxidation of methane on VO_x/SiO_2 (Fig. 10). The vanadium species is an isolated vanadyl with three bridging siloxy bonds to the surface, as well established [35,42,43,44]. Interaction with a gas

phase NO_2 molecule produces a monodentate nitrate species which is the predominant adsorbed form with a characteristic band at 1363 cm^{-1}. One possibility for reaction is for the monodentate nitrate to rearrange to a reactive bidentate nitrate (Fig. 10). This species can add methane, simultaneously releasing NO, which likely drives the reaction energetically. The resulting methoxy species can undergo α-hydride elimination to vanadium and through electron rearrangement to form formaldehyde. In a final step the catalytic center would be reoxidized by an oxygen equivalent, possibly derived from the reaction of two adjacent reduced vanadyl groups (not shown). The suggested pathway involves standard organometallic reactions and is reasonable for several reasons: a) there is formation of a methoxy group rather than a methyl group (C-O-M groups are more likely to yield selective oxidation products than C-M groups [89]), b) the methoxy group that is formed binds to a vanadium center rather to a siloxy group (leading to facile α-elimination), c) an OH group is formed on Si (leading to facile H_2O formation), d) the known chemistry of VO_x occurs because the oxygen involved in formaldehyde formation is a lattice oxygen atom (not adsorbed oxygen). Note that monodentate nitrate could form on the bridging oxygen atom not the terminal oxygen atom and a similar sequence of steps could be derived. It should also be recognized that this is by no means the only possible reaction route. For example, the nitrate could react with methane by abstracting a hydrogen atom and producing a methyl radical. Nevertheless, the suggested sequence provides an accounting of the major results of this study and is consistent with past results from the literature.
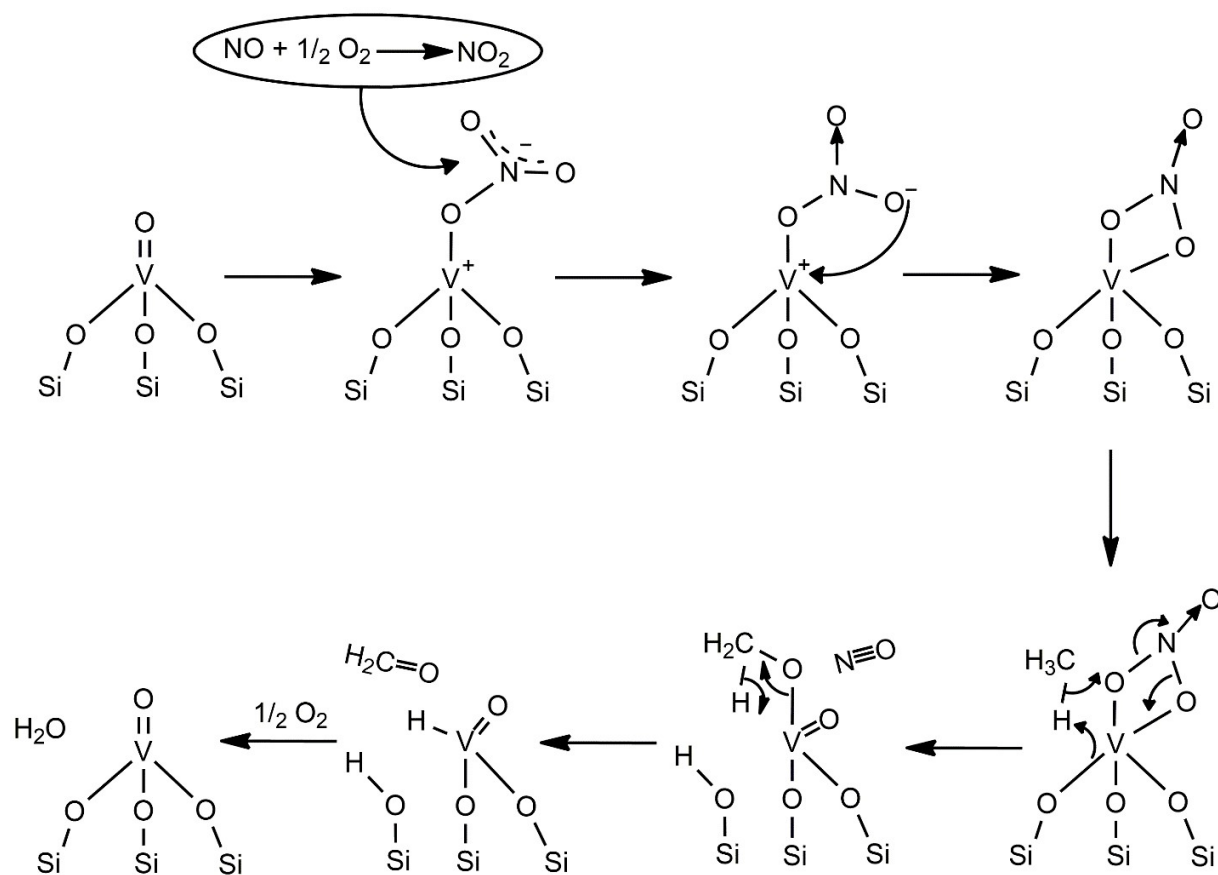
Fig. 10. Possible scheme for the formation of HCHO during the CH_4 partial oxidation by $NO + O_2$ involving the terminal V=O bond and the Si-O-V bond

4.   **Conclusions**

Methane oxidation using either O_2 or an $NO+O_2$ mixture as oxidants was studied over a

series of transition metal oxides (VO_x, CrO_x, MnO_x, NbO_x, MoO_x, and WO_x) supported on silica

at atmospheric pressure and temperatures ranging from 300 to 400 °C. Raman spectroscopy and

oxygen chemisorption indicated that the metal oxides were in a highly dispersed state on the

silica support. Negligible CH_4 conversion was obtained using only O_2 on all of the catalysts

except for Mn, which reflected the difficulty of O_2 dissociation at these conditions. Conversely, detectable CH_4 conversion was observed using the $NO+O_2$ mixture on all catalysts. This was rationalized by an NO-mediated O_2 dissociation process through the facile formation of NO_2. In situ FTIR spectroscopy indicated that the reaction proceeded through the formation of a monodentate nitrate species, which may have originated from an interaction between adsorbed NO_2 and a surface oxygen atom from the metal oxide (probably O^{2-}). The surface nitrate species were the likely reactive intermediates to functionalize methane. The product selectivities from temperature-dependent reactivity measurements were consistent with the known chemistry of the metal oxides: the oxides of chromium, manganese, and niobium gave selectivity to only CO_2, whereas the oxides of vanadium, molybdenum, and tungsten gave selectivity to CO_2 and HCHO. Contact time measurements with representative samples for partial oxidation (VO_x/SiO_2) and complete oxidation (MnO_x/SiO_2) gave further evidence of their intrinsic oxidation properties.

Acknowledgements

References

[1]   J. Haber, Catalytic oxidation -State of the art and prospects, in: P. Ruiz, B. Delmon (Eds.) New Development in Selective Oxidation by Heterogeneous Catalysis, Stud. Surf. Sci. Catal. 72, Elsevier, 1992, pp. 279-304.

[2]   R.K. Grasselli, J.D. Burrington, Selective Oxidation and Ammoxidation of Propylene by Heterogeneous Catalysis, in: D.D. Eley, H. Pines, P.B. Weisz (Eds.) Adv. Catal. 30, Academic Press, 1981, pp. 133-163.

[3]   F. Cavani, Catalytic selective oxidation: The forefront in the challenge for a more sustainable chemical industry, Catal. Today 157 (2010) 8-15.

[4]   S.T. Oyama, Factors affecting selectivity in catalytic partial oxidation and combustion reactions, in: B.K. Warren, S.T. Oyama (Eds.) Heterogeneous Hydrocarbon Oxidation ACS Symp. Series 638, Washington DC, 1996, pp. 2-19.

[5]   J. Haber, Selectivity in heterogeneous catalytic oxidation, in: B.K. Warren, S.T. Oyama (Eds.) Heterogeneous Hydrocarbon Oxidation, ACS Symp. Series 638, Washington DC, 1996, pp. 20-35.

[6]   S.T. Oyama, A.N. Desikan, J.W. Hightower, Research challenges in selective oxidation, in: S.T. Oyama, J.W. Hightower (Eds.) Catalytic Selective Oxidation, ACS Symp. Series 523, Washington, DC, 1993, pp. 1-15

[7]   R.K. Grasselli, Fundamental principles of selective heterogeneous oxidation catalysis, Top. Catal. 21 (2002) 79-88.

[8]   R.K. Grasselli, Site isolation and phase cooperation: Two important concepts in selective oxidation catalysis: A retrospective, Catal. Today 238 (2014) 10-27.

[9]   R.K. Grasselli, Advances and future trends in selective oxidation and ammoxidation catalysis, Catal. Today 49 (1999) 141-153.

[10]   A. Bielański, J. Haber, Oxygen in catalysis on transition metal oxides, Catal. Rev.–Sci. Eng. 19 (1979) 1-41.

[11]   A. Bielański, J. Haber, Oxygen in Catalysis, CRC Press, Boca Raton, 1991.

[12]   J. Lu, J. J. Bravo-Suárez, M. Haruta, S. T. Oyama, Direct propylene epoxidation over modified $Ag/CaCO_3$ catalysts, Appl. Catal. A: Gen. 302 (2006) 283-295.

[13]   J. Haber, W. Turek, Kinetic studies as a method to differentiate between oxygen species involved in the oxidation of propene, J. Catal. 190 (2000) 320-326.

[14]   J.M. Libre, Y. Barbaux, B. Grzybowska, J.P. Bonnelle, A surface potential study of adsorbed oxygen species on a $Bi_2Mo_3O_{12}$ catalyst, React. Kinet. Catal. Lett. 20 (1982) 249-254.

[15]   J.M. Libre, Y. Barbaux, B. Grzybowska, P. Gonflant, J.P. Bonnelle, Catalytic oxidation of propene: Surface potential measurements and structural properties of α-$Bi_2Mo_3O_{12}$, α-Bi_2O_3 and MoO_3, Appl. Catal. 6 (1983) 315-328.

[16]   M.A. Bañares, A. Guerrero-Ruiz, I. Rodríguez-Ramos, J.L.G. Fierro, Mechanistic aspects of the selective oxidation of methane to C_1-oxygenates over MoO_3/SiO_2 catalysts in a single catalytic step, in: L. Guczi, F. Solymosi, P. Tétényi (Eds.) New Frontiers in Catalysis, Elsevier, Amsterdam, 1993, pp. 1132-1140.

[17]   N.D. Spencer, C.J. Pereira, R.K. Grasselli, The effect of sodium on the MoO_3-SiO_2-catalyzed partial oxidation of methane, J. Catal. 126 (1990) 546-554.

[18]   M.A. Bañares, J.L.G. Fierro, Methane-selective oxidation of silica-supported molybdenum(VI) catalysts, in: S.T. Oyama, J.W. Hightower (Eds.) Catalytic Selective Oxidation, ACS Symp. Series 523, Washington, DC, 1993, pp. 354-367.

[19]   K. Suzuki, T. Hayakawa, M. Shimizu, K. Takehira, Partial oxidation of methane over silica supported molybdenum oxide catalysts, Catal. Lett. 30 (1994) 159-169.

[20]   M.M. Koranne, J.G. Goodwin Jr., G. Marcelin, Partial oxidation of methane over silica- and alumina- supported vanadia catalysts, J. Catal. 148 (1994) 388-391.

[21]   K.J. Zhen, M.M. Khan, C.H. Mak, K.B. Lewis, G.A. Somorjai, Partial oxidation of methane with nitrous oxide over V_2O_5-SiO_2 catalyst, J. Catal. 94 (1985) 501-507.

[22]   N.D. Spencer, C.J. Pereira, V_2O_5-SiO_2-catalyzed methane partial oxidation with molecular oxygen, J. Catal. 116 (1989) 399-406.

[23]   T.T.H. Dang, D. Seeburg, J. Radnik, C. Kreyenschulte, H. Atia, T.T.H. Vu, S. Wohlrab, Influence of V-sources on the catalytic performance of VMCM-41 in the selective oxidation of methane to formaldehyde, Catal. Commun. 103 (2018) 56-59.

[24]   A.J. Marchi, E.J. Lede, F.G. Requejo, M. Rentería, S. Irusta, E.A. Lombardo, E.E. Miró, Laser Raman spectroscopy (LRS) and time differential perturbed angular correlation (TDPAC) study of surface species on Mo/SiO_2 and $Mo,Na/SiO_2$. Their role in the partial oxidation of methane, Catal. Lett. 48 (1997) 47-54.

[25]   M. A. Bañares, J. H. Cardoso, G. J. Hutchings, J. M. Correa Bueno, J. L.G. Fierro, Selective oxidation of methane to methanol and formaldehyde over V_2O_5/SiO_2 catalysts. Role of NO in the gas phase, Catal. Lett. 1998 (56) 149-153.

[26]   J.A. Barbero, M.C. Alvarez, M.A. Bañares, M.A. Peña, J.L.G. Fierro, Breakthrough in the direct conversion of methane into C_1-oxygenates, Chem. Commun. (2002) 1184-1185.

[27]   T. Takemoto, K. Tabata, Y. Teng, L.-X. Dai, E. Suzuki, Selective oxidation of methane in CH_4–O_2–NO_2 over MoO_3, Catal. Today 71 (2001) 47-53.

[28]   T. Takemoto, D. He, Y. Teng, K. Tabata, E. Suzuki, The optimization of methanol yield in direct selective oxidation of methane with O_2 and NO in the presence of Cu-ZnO/Al_2O_3, J. Mol. Catal. A: Chem. 179 (2002) 279-286.

[29]   T. Takemoto, D. He, Y. Teng, A. Nakayama, K. Tabata, E. Suzuki, Enhancement of methanol selectivity in the products of direct selective oxidation of methane in CH_4–O_2–NO with Cu–ZnO/Al_2O_3, J. Catal. 198 (2001) 109-115.

[30]   V. Vargheese, J. Murakami, K.K. Bando, I.T. Ghampson, G.-N. Yun, Y. Kobayashi, S.T. Oyama, The direct molecular oxygen partial oxidation of CH_4 to dimethyl ether without methanol formation over a Pt/Y_2O_3 catalyst using an NO/NO_2 oxygen atom shuttle, J. Catal. 389 (2020) 352-365.

[31]   V. Vargheese, Y. Kobayashi, S.T. Oyama, The direct partial oxidation of methane to dimethyl ether over Pt/Y_2O_3 catalysts using an NO/O_2 shuttle, Angew. Chem. Int. Ed. 59 (2020) 16644-16650.

[32]   I. T. Ghampson, S.-T. B. Lundin, T. Shishido, S. T. Oyama, Isotopic $^{18}O/^{16}O$ substitution study on the direct partial oxidation of CH_4 to dimethyl ether over a Pt/Y_2O_3 catalyst using NO/O_2 as an oxidant, Catal. Sci. Technol. 11 (2021) 2708-2712

[33]   H. Gershinowitz, H. Eyring, The theory of trimolecular reactions, J. Am. Chem. Soc. 57 (1935) 985-991.

[34]   A.N. Desikan, L. Huang, S.T. Oyama, Oxygen chemisorption and laser Raman spectroscopy of unsupported and silica-supported molybdenum oxide, J. Phys. Chem. 95 (1991) 10050-10056.

[35]   S.T. Oyama, G.T. Went, K.B. Lewis, A.T. Bell, G.A. Somorjai, Oxygen chemisorption and laser Raman spectroscopy of unsupported and silica-supported vanadium oxide catalysts, J. Phys. Chem. 93 (1989) 6786-6790.

[36]   G. T. Went, S. T. Oyama and A. T. Bell, Oxygen chemisorption and laser Raman spectroscopy of vanadium oxide supported on silica, alumina, and titania, J. Phys. Chem. 94 (1990) 4240-4246.

[37] C. Reed, Y. Xi, S. T. Oyama, Distinguishing between reaction intermediates and spectators: A kinetic study of acetone oxidation using ozone on a silica-supported manganese oxide catalyst, J. Catal. 235 (2005) 378-392.

[38] R.L. McCreery, Raman Spectroscopy for Chemical Analysis, John Wiley & Sons, Inc., Hoboken, NJ, 2000.

[39] A. Khodakov, B. Olthof, A.T. Bell, E. Iglesia, Structure and catalytic properties of supported vanadium oxides: Support effects on oxidative dehydrogenation reactions, J. Catal. 181 (1999) 205-216.

[40] C. Reed, Y.-K. Lee, S.T. Oyama, Structure and oxidation state of silica-supported manganese oxide catalysts and reactivity for acetone oxidation with ozone, J. Phys. Chem. B 110 (2006) 4207-4216.

[41] J.M. Jehng, H.C. Hu, X.T. Gao, I.E. Wachs, The dynamic states of silica-supported metal oxide catalysts during methanol oxidation, Catal. Today 28 (1996) 335-350.

[42] R. Chlosta, G. Tzolova-Müller, R. Schlögl, C. Hess, Nature of dispersed vanadium oxide: influence of the silica support structure and synthesis methods, Catal. Sci. Technol. 1 (2011) 1175-1181.

[43] T. Fu, Y. Wang, A. Wernbacher, R. Schlögl, A. Trunschke, Single-site vanadyl species isolated within molybdenum oxide monolayers in propane oxidation, ACS Catal. 9 (2019) 4875-4886.

[44] C. Moisii, L.J. van de Burgt, A.E. Stiegman, Resonance Raman spectroscopy of discrete silica-supported vanadium oxide, Chem. Mater. 20 (2008) 3927-3935.

[45] C. Moisii, M.D. Curran, L.J. van de Burgt, A.E. Stiegman, Raman spectroscopy of discrete silica supported vanadium oxide: assignment of fundamental stretching modes, J. Mater. Chem. 15 (2005) 3519-3524.

[46] D. Maganas, A. Trunschke, R. Schlögl, F. Neese, A unified view on heterogeneous and homogeneous catalysts through a combination of spectroscopy and quantum chemistry, Faraday Discuss. 188 (2016) 181-197.

[47] D. Kim, J.-M. Tatibouet, I.E. Wachs, Surface structure and reactivity of CrO_3/SiO_2 catalysts, J. Catal. 136 (1992) 209-221.

[48]   C. Moisii, D. Jeffcoat, N. Peek, L. van de Burgt, S.L. Scott, A.E. Stiegman, Do mono-oxo sites exist in silica-supported Cr(VI) materials? Reassessment of the resonance Raman spectra, J. Phys. Chem. C 122 (2018) 17149-17160.

[49]   J. Handzlik, R. Grybos, F. Tielens, Structure of monomeric chromium(VI) oxide species supported on silica: Periodic and cluster DFT studies, J. Phys. Chem. C 117 (2013) 8138-8149.

[50]   G. Koch, M. Hävecker, D. Teschner, S.J. Carey, Y. Wang, P. Kube, W. Hetaba, T. Lunkenbein, G. Auffermann, O. Timpe, F. Rosowski, R. Schlögl, A. Trunschke, Surface conditions that constrain alkane oxidation on perovskites, ACS Catal. 10 (2020) 7007-7020.

[51]   X. Li, D. Teschner, V. Streibel, T. Lunkenbein, L. Masliuk, T. Fu, Y. Wang, T. Jones, F. Seitz, F. Girgsdies, F. Rosowski, R. Schlögl, A. Trunschke, How to control selectivity in alkane oxidation?, Chem. Sci. 10 (2019) 2429-2443.

[52]   F. Buciuman, F. Patcas, R. Craciun, D.R.T. Zahn, Vibrational spectroscopy of bulk and supported manganese oxides, Phys. Chem. Chem. Phys. 1 (1999) 185-190.

[53]   J.M. Jehng, I.E. Wachs, Molecular design of supported niobium oxide catalysts, Catal. Today, 16 (1993) 417-426.

[54]   K. Amakawa, L. Sun, C. Guo, M. Havecker, P. Kube, I.E. Wachs, S. Lwin, A.I. Frenkel, A. Patlolla, K. Hermann, R. Schlogl, A. Trunschke, How strain affects the reactivity of surface metal oxide catalysts, Angew. Chem. Int. Ed. 52 (2013) 13553-13557.

[55]   K. Kurleto, F. Tielens, J. Handzlik, Isolated molybdenum(VI) and tungsten(VI) oxide species on partly dehydroxylated silica: A computational perspective, J. Phys. Chem. C 124 (2020) 3002-3013.

[56]   D.S. Kim, M. Ostromecki, I.E. Wachs, S.D. Kohler, J.G. Ekerdt, Preparation and characterization of WO_3/SiO_2 catalysts, Catal. Lett. 33 (1995) 209-215.

[57]   R.M. Navarro, M.A. Peña, J.L.G. Fierro, Methane oxidation on metal oxides, in: J.L.G. Fierro (Ed.) Metal Oxides- Chemistry and Applications, CRC Press, Taylor & Francis, Boca Raton, 2006, pp. 463-490.

[58]   S.H. Taylor, J.S.J. Hargreaves, G.J. Hutchings, R.W. Joyner, C.W. Lembacher, The partial oxidation of methane to methanol: An approach to catalyst design, Catal. Today 42 (1998) 217-224.

[59]   S. T. Oyama, W. Li, W. Zhang, A comparative study of ethanol oxidation with ozone on supported Mo and Mn catalysts, Science and Technology in Catalysis Kodansha, Tokyo, 1999, pp. 105-110.

[60]   M.A. Bañares, L.J. Alemany, F. Martin-Jiménez, J.M. Blasco, M.L. Granados, M.A. Peña, J.L.G. Fierro, Partial oxidation of methane on low-surface-area SiO_2-Si-supported vanadia catalysts, in: B.K. Warren, S.T. Oyama (Eds.) Heterogeneous Hydrocarbon Oxidation ACS Symp. Series 638, Washington DC, 1996, pp. 78-94.

[61]   M. Bodenstein, Lindner, Bildung und zersetzung der höheren stickoxyde, Z. Physik. Chem. 87 (1922) 100.

[62]   H. Gershinowitz, H. Eyring, The Theory of trimolecular reactions, J. Am. Chem. Soc. 57 (1935) 985–991.

[63]   R. Mauti, C.A. Mims, Oxygen pathways in methane selective oxidation over silica-supported molybdena, Catal. Lett. 21 (1993) 201-207.

[64]   Y. Wu, J. Chen, W. Hu, K. Zhao, P. Qu, P. Shen, M. Zhao, L. Zhong, Y. Chen, Phase transformation and oxygen vacancies in Pd/ZrO_2 for complete methane oxidation under lean conditions, J. Catal. 377 (2019) 565-576.

[65]   A. Iino, A. Cho, A. Takagaki, R.Kikuchi, S. T. Oyama, Kinetic studies of HDO of 2-methyl-tetrahydrofuran on a Ni_2P/SiO_2 catalyst, J. Catal. 311 (2014)17–27.

[66]   G.-N. Yun, T. I. Ghampson, W. Movick, V. Vargheese, Y. Kobayashi, S. T. Oyama, Applicability of the Delplot method for the determination of catalytic reaction sequences: Hydrodeoxygenation of γ-valerolactone on $Ni_2P/MCM-41$, Chem. Eng. Sci. 223 (2020) 115697.

[67]   M. Ravi, M. Ranocchiari, J. A. van Bokhoven, The direct catalytic oxidation of methane to methanol a critical assessment, Angew. Chem. Int. Ed. 56 (2017)16464 – 16483.

[68]   A.R. Kulkarni, Z.-J. Zhao, S. Siahrostami, J.K. Nørskov, F. Studt, Cation-exchanged zeolites for the selective oxidation of methane to methanol, Catal. Sci. Technol. 8 (2018) 114-123.

[69]   E. Yang, J.G. Lee, D.H. Kim, Y.S. Jung, J.H. Kwak, E.D. Park, K. An, $SiO_2@V_2O_5@Al_2O_3$ core–shell catalysts with high activity and stability for methane oxidation to formaldehyde, J. Catal. 368 (2018) 134-144.

[70]   X. Wang, Y. Wang, Q. Tang, Q. Guo, Q. Zhang, H. Wan, MCM-41-supported iron phosphate catalyst for partial oxidation of methane to oxygenates with oxygen and nitrous oxide, J. Catal. 217 (2003) 457-467.

[71]   H.F. Liu, R.S. Liu, K.Y. Liew, R.E. Johnson, J.H. Lunsford, Partial oxidation of methane by nitrous oxide over molybdenum on silica, J. Am. Chem. Soc. 106 (1984) 4117-4121.

[72]   E.M. Alayon, M. Nachtegaal, M. Ranocchiari, J.A. van Bokhoven, Catalytic conversion of methane to methanol over Cu–mordenite, Chem. Commun. 48 (2012) 404-406.

[73]   B.E.R. Snyder, P. Vanelderen, M.L. Bols, S.D. Hallaert, L.H. Böttger, L. Ungur, K. Pierloot, R.A. Schoonheydt, B.F. Sels, E.I. Solomon, The active site of low-temperature methane hydroxylation in iron-containing zeolites, Nature 536 (2016) 317.

[74]   C. Hammond, M.M. Forde, M.H. Ab Rahim, A. Thetford, Q. He, R.L. Jenkins, N. Dimitratos, J.A. Lopez-Sanchez, N.F. Dummer, D.M. Murphy, A.F. Carley, S.H. Taylor, D.J. Willock, E.E. Stangland, J. Kang, H. Hagen, C.J. Kiely, G.J. Hutchings, Direct catalytic conversion of methane to methanol in an aqueous medium by using copper-promoted Fe-ZSM-5, Angew. Chem. Int. Ed. 124 (2012) 5219-5223.

[75]   N. Agarwal, S.J. Freakley, R.U. McVicker, S.M. Althahban, N. Dimitratos, Q. He, D.J. Morgan, R.L. Jenkins, D.J. Willock, S.H. Taylor, C.J. Kiely, G.J. Hutchings, Aqueous Au-Pd colloids catalyze selective CH_4 oxidation to CH_3OH with O_2 under mild conditions, Science 358 (2017) 223-227.

[76]   M.V. Parfenov, E.V. Starokon, L.V. Pirutko, G.I. Panov, Quasicatalytic and catalytic oxidation of methane to methanol by nitrous oxide over FeZSM-5 zeolite, J. Catal. 318 (2014) 14-21.

[77]   K.S. Park, J.H. Kim, S.H. Park, D.J. Moon, H.-S. Roh, C.-H. Chung, S.H. Um, J.-H. Choi, J.W. Bae, Direct activation of CH_4 to oxygenates and unsaturated hydrocarbons using N_2O on Fe-modified zeolites, J. Mol. Catal. A: Chem. 426 (2017) 130-140.

[78]   B. Ipek, R. F. Lobo, Catalytic conversion of methane to methanol on Cu-SSZ-13 using N_2O as oxidant, Chem. Commun. 52 (2016) 13401-13404.

[79]   J. Xu, R.D. Armstrong, G. Shaw, N.F. Dummer, S.J. Freakley, S.H. Taylor, G.J. Hutchings, Continuous selective oxidation of methane to methanol over Cu- and Fe-modified ZSM-5 catalysts in a flow reactor, Catal. Today 270 (2016) 93-100.

[80]   V.D.B.C. Dasireddy, D. Hanzel, K. Bharuth-Ram, B. Likozar, The effect of oxidant species on direct, non-syngas conversion of methane to methanol over an $FePO_4$ catalyst material, RSC Adv. 9 (2019) 30989-31003.

[81]   W. Li, S.T. Oyama, Catalytic methane oxidation at low temperatures using ozone, in: B.K. Warren, S.T. Oyama (Eds.) Heterogeneous Hydrocarbon Oxidation ACS Symp. Series 638, Washington DC, 1996, pp 364-373.

[82]   K.I. Hadjiivanov, Identification of neutral and charged N_xO_y surface species by IR spectroscopy, Catal. Rev.–Sci. Eng. 42 (2000) 71-144.

[83]   M.Y. Mihaylov, V.R. Zdravkova, E.Z. Ivanova, H.A. Aleksandrov, P.S. Petkov, G.N. Vayssilov, K.I. Hadjiivanov, Infrared spectra of surface nitrates: Revision of the current opinions based on the case study of ceria, J. Catal. 394 (2021) 245-258.

[84]   N. Tang, Y. Liu, H. Wang, Z. Wu, Mechanism study of NO catalytic oxidation over MnO_x/TiO_2 catalysts, J. Phys. Chem. C 115 (2011) 8214-8220.

[85]   U. Bentrup, A. Brückner, M. Richter, R. Fricke, NOx adsorption on MnO_2/NaY composite: An in situ FTIR and EPR study, Appl. Catal. B: Environ. 32 (2001) 229-241.

[86]   C. Yu, B. Huang, L. Dong, F. Chen, X. Liu, In situ FT-IR study of highly dispersed $MnO_x/SAPO-34$ catalyst for low-temperature selective catalytic reduction of NO_x by NH3, Catal. Today 281 (2017) 610-620.

[87]   B. Djonev, B. Tsyntsarski, D. Klissurski, K. Hadjiivanov, IR spectroscopic study of NO adsorption and NO–O_2 coadsorption on Co^{2+}/SiO_2 catalysts, J. Chem. Soc. Faraday Trans. 93 (1997) 4055-4063.

[88]   S.T. Oyama, Structure and reactivity of silica-supported vanadium oxide, Res. Chem. Intermed. 15 (1991) 165-182.

[89]   S.T. Oyama, Adsorbate bonding and the selection of partial and total oxidation pathways, J. Catal. 128 (1991) 210-217.